ARTICLE

SWI2/SNF2 ATPase CHR2 remodels pri-miRNAs via Serrate to impede miRNA production

Zhiye Wang^{1,2}, Zeyang Ma^{1,2,5}, Claudia Castillo-González^{1,2,5}, Di Sun^{1,2}, Yanjun Li^{1,2,3}, Bin Yu⁴, Baoyu Zhao¹, Pingwei Li¹ & Xiuren Zhang^{1,2}*

Chromatin remodelling factors (CHRs) typically function to alter chromatin structure. CHRs also reside in ribonucleoprotein complexes, but little is known about their RNA-related functions. Here we show that CHR2 (also known as BRM), the ATPase subunit of the large switch/sucrose non-fermentable (SWI/SNF) complex, is a partner of the Microprocessor component Serrate (SE). CHR2 promotes the transcription of primary microRNA precursors (primiRNAs) while repressing miRNA accumulation in vivo. Direct interaction with SE is required for post-transcriptional inhibition of miRNA accumulation by CHR2 but not for its transcriptional activity. CHR2 can directly bind to and unwind pri-miRNAs and inhibit their processing, and this inhibition requires the remodelling and helicase activity of CHR2 in vitro and in vivo. Furthermore, the secondary structures of pri-miRNAs differed between wild-type *Arabidopsis thaliana* and *chr2* mutants. We conclude that CHR2 accesses pri-miRNAs through SE and remodels their secondary structures, preventing downstream processing by DCL1 and HYL1. Our study uncovers pri-miRNAs as a substrate of CHR2, and an additional regulatory layer upstream of Microprocessor activity to control miRNA accumulation.

CHR2 is the ATPase subunit of the large SWI/SNF chromatin-remodelling complex. Such complexes are known to remodel chromatin structures by nucleosome sliding, eviction, or histone variant exchange using energy derived from ATP hydrolysis¹. Animal CHR2 can also associate with nascent mRNA ribonucleoprotein complexes (pre-mRNPs)².³. The yeast chromatin remodeller ISW1 is involved in the surveillance of nuclear mRNP biogenesis⁴. Some SWI/SNF members can also bind to long-noncoding RNAs (lncRNAs) and participate in assembly of lncRNA-dependent nuclear bodies or regulation of chromatin association⁵-8. These studies suggest that CHR2 and other SWI/SNF subunits have additional roles in RNA biology. Notably, these roles do not require the remodelling activity of the relevant ATPases. Whether and how SWI/SNF factors participate in post-transcriptional processing of RNA is unknown.

MicroRNAs, a large family of small non-coding regulatory RNAs⁹, are processed from long pri-miRNAs that contain a hairpin-like foldback by Microprocessor and Dicing complexes^{10,11}. The minimal plant Microprocessor–Dicing complex includes Dicer-like 1 (DCL1), and a double-stranded (ds)RNA-binding protein, Hyponastic leaves 1 (HYL1)¹². The Microprocessor initially cleaves basal flanking segments of pri-miRNAs to generate precursor miRNAs (pre-miRNAs), and subsequently cuts pre-miRNAs to produce miRNA/* duplexes (where the asterisk represents a miRNA complementary strand)¹³. Although miRNAs are derived from pri-miRNAs, transcript levels of pri-miRNAs do not always correlate with miRNA abundance, possibly owing to various post-transcriptional regulations and processing efficiencies of the RNA species^{12,14,15}.

SE, a zinc-finger protein, has also been considered to be a core component of plant Microprocessor, because *se* mutations cause pri-miRNA accumulation and miRNA loss in vivo¹⁶. Although some have argued for a direct role for SE in promoting the enzymatic activity

and accuracy of DCL1 17,18 , processing of pri-miRNAs by DCL1 in vitro does not seem to require SE 12 ; rather, SE might act as a scaffold to recruit the processing machinery including DCL1 and HYL1 to proper RNA substrates to produce miRNAs *in vivo* 12,19,20 . Ars2, the mammalian orthologue of SE, also participates in miRNA-dependent silencing, suggesting that the function of SE has been conserved throughout eukaryotes 21,22 . However, the mechanism by which SE contributes to miRNA production has been unclear.

CHR2 has two roles in miRNA accumulation

We identified CHR2 as a bona fide partner of SE (Fig. 1a, b, Extended Data Fig. 1a–d, Supplementary Information). We then investigated whether CHR2 participated in SE-mediated miRNA production. Adult chr2-1 mutant plants exhibited short stature and downward curled leaves, whereas se mutants had small serrated and upward curled leaves (Extended Data Fig. 1e, f). Small RNA (sRNA) blot assays showed that the amounts of the tested miRNAs, except miR390, were greatly increased in leaves and flowers of $chr2-1^{-/-}$ compared to wild-type (Col-0) plants or their heterozygote siblings $(chr2-1^{+/-})$ (Fig. 1c, Extended Data Fig. 1g–i). Moreover, both morphological and miRNA abnormalities in chr2-1 plants were fully complemented by a PCHR2-gCHR2-Flag-4Myc (PCHR2-gCHR2-FM) transgene, showing that the lack of CHR2 causes both morphological and miRNA abnormalities (Extended Data Fig. 1j, k).

We compared miRNA profiles in *chr2-1* and Col-0 plants through deep-sequencing analysis. We normalized sequencing read counts to miR390, which consistently showed no changes between *chr2-1* and Col-0 plants in either sRNA blots or sequencing (see Methods). We found that 114 of 365 annotated miRNAs were upregulated at least 1.5-fold in *chr2-1* relative to Col-0 plants (Fig. 1d, Supplementary Table 1). We focused on the 259 canonical SE-dependent miRNAs and

¹Department of Biochemistry and Biophysics, Texas A&M University, College Station, TX, USA. ²Institute for Plant Genomics and Biotechnology, Texas A&M University, College Station, TX, USA.

³College of Plant Protection, Nanjing Agricultural University, Nanjing, China. ⁴School of Biological Sciences & Center for Plant Science Innovation, University of Nebraska-Lincoln, Lincoln, NE, USA.

⁵These authors contributed equally: Zeyang Ma, Claudia Castillo-González. *e-mail: xiuren.zhang@tamu.edu

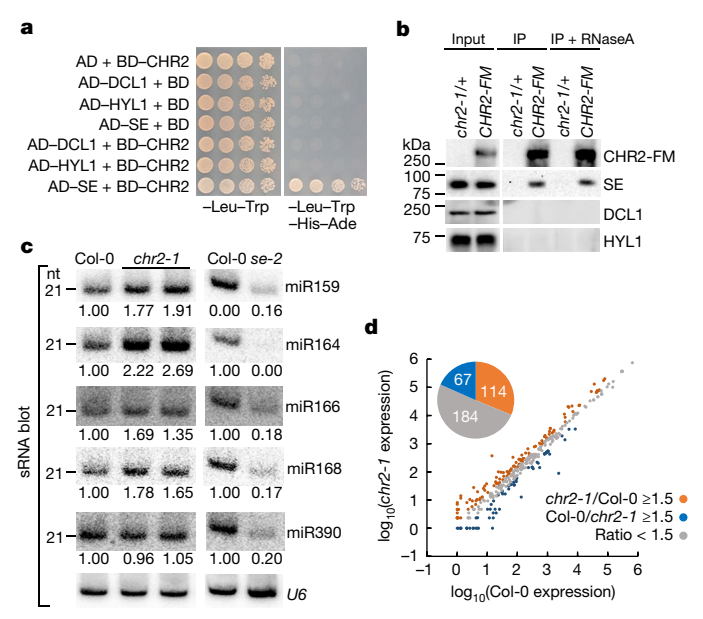


Fig. 1 | CHR2 is a novel partner of SE and represses miRNA accumulation. a, b, Y2H (a) and co-immunoprecipitation (IP) (b) assays show the specific CHR2–SE interaction. AD, GAL4-activation domain; BD, GAL4-DNA-binding domain; AD or BD-protein, AD or BD-fusion proteins; CHR2-FM, chr2-1; PCHR2-gCHR2-Flag-4Myc. c, sRNA blot analysis shows that miRNAs accumulated in chr2-1 mutant plants. d, sRNA sequencing analysis shows that a substantial number of miRNAs accumulated in chr2-1 mutants. Compared to Col-0, miRNAs with at least 1.5-fold higher (chr2-1/Col-0 \geq 1.5) or lower (Col-0/chr2-1 \geq 1.5) expression in chr2-1 are indicated by orange dots and blue dots, respectively. The grey dots indicate differences in expression level < 1.5-fold (ratio < 1.5).

found that approximately one-quarter of these SE-dependent miRNAs, representing about 59% of CHR2-repressed miRNAs, were significantly enhanced in *chr2-1* plants (Extended Data Fig. 1l, m, Supplementary Table 1). Thus, CHR2 is a previously unrecognized negative regulator of miRNA accumulation for a large subset of miRNAs in *Arabidopsis*.

We then investigated the transcription levels of miRNA genes (MIRs) in *chr2* mutants through *PMIR-FM-GUS* reporter assays and measurement of nascent pri-miRNA levels. Notably, unlike the effects on miRNA accumulation, MIR gene transcription was reduced in *chr2* mutants (Extended Data Fig. 2, Supplementary Table 2, Supplementary Information). Thus, CHR2 must have an additional inhibitory role in miRNA biogenesis, beyond its canonical function in promoting MIR transcription.

Uncoupled CHR2 roles in miRNA biogenesis

To study whether the functions of CHR2 in miRNA biogenesis depend on SE, we mapped the CHR2–SE interaction interface. Using yeast two-hybrid (Y2H) assays with dozens of CHR2 mutants, we found that CHR2(E1747A) abolished the CHR2–SE interaction (Fig. 2a, Extended Data Fig. 3a–e, Supplementary Information). Thus, E1747 of CHR2 is essential for the specific CHR2–SE interaction. We then transformed *PCHR2-gCHR2(E1747A)-FM* into *chr2-1* plants and obtained T2 homozygotes. Notably, CHR2(E1747A) only partially rescued the morphological and miRNA defects in *chr2-1* plants (Fig. 2b, c). This result indicated that the direct CHR2–SE interaction is required for inhibition of miRNA accumulation in vivo by CHR2.

Through genetic crossing, we obtained *chr2-1;PCHR2-gCHR2* (E1747A)-FM;PMIR159a-FM-GUS homozygotes. The expression level of the GUS reporter was comparable in *chr2-1;PCHR2-gCHR2* (E1747A)-FM and Col-0 backgrounds (Fig. 2d, Extended Data Fig. 3f). Thus, the E1747A mutation does not alter the transcriptional function of CHR2. This result also suggests that enhanced miRNA accumulation in the *chr2-1;PCHR2-gCHR2*(E1747A)-FM hypomorphic line results

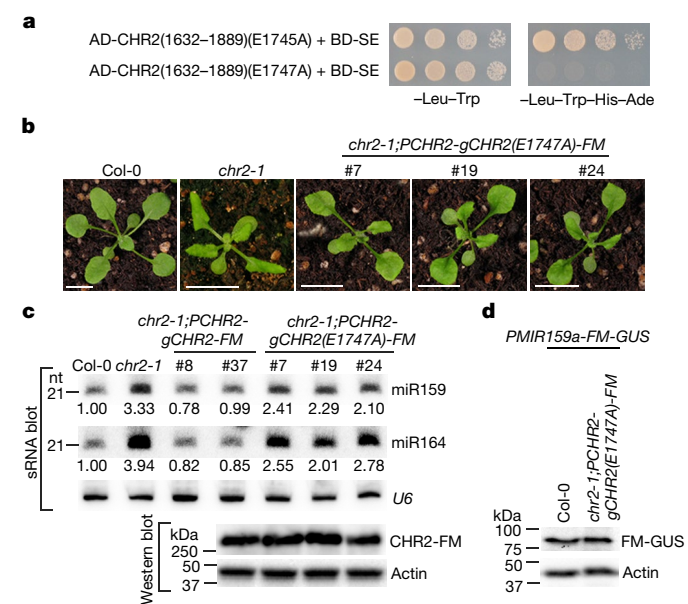


Fig. 2 | Uncoupling of transcriptional and post-transcriptional regulatory roles of CHR2 in miRNA biogenesis. a, Y2H assay shows that CHR2(E1747) is required for its interaction with SE. b, c, CHR2(E1747A) partially rescued the morphological and miRNA accumulation defects seen in *chr2-1* plants. b, Scale bars, 1 cm. c, sRNA blot analysis (top) and western blot analysis of CHR2 or its variant (bottom). d, Western blot analysis of GUS protein from *PMIR159a-FM-GUS* homozygotes show that CHR2(E1747A) does not alter the transcriptional level of *MIR159a* in Col-0 and *chr2-1;PCHR2-gCHR2(E1747A)-FM* backgrounds (n > 30).

from compromised inhibition of SE-mediated miRNA biogenesis by CHR2(E1747A). Thus, the transcriptional and post-transcriptional regulatory roles of CHR2 in miRNA biogenesis can be uncoupled via SE.

CHR2 inhibits pri-miRNA processing in vitro

CHR2 does not affect the expression of miRNA metabolism components or SE-dependent pre-mRNA splicing (Extended Data Fig. 4, Supplementary Table 3, Supplementary Information). To test whether CHR2 directly inhibits SE-mediated pri-miRNA processing, we established an in vitro Microprocessor system using recombinant DCL1, SE, and HYL1. The recombinant Microprocessor (DCL1-HYL1-SE) cleaved pri-miR166f as efficiently and accurately as DCL1 immunoprecipitates from plants¹² (Extended Data Fig. 5a, b). Thus, the recombinant Microprocessor can recapitulate in vivo miRNA biogenesis. Notably, incubation of purified CHR2, but not a control (hSTING)²³, with pri-miRNAs before application of HYL1-SE substantially inhibited Microprocessor activity (Fig. 3a, Extended Data Fig. 5c). CHR2-mediated inhibition of Microprocessor activity was concentrationdependent and also enhanced by prolonged incubation with pri-miRNA (Extended Data Fig. 5d, e). By contrast, treatment with CHR2 after pri-miRNA incubation with HYL1-SE only slightly inhibited DCL1 activity (Fig. 3b, Extended Data Fig. 5f). Thus, Microprocessor, when loaded with pri-miRNAs, could largely bypass CHR2 inhibition in vitro. This result also suggests that CHR2 impedes miRNA biogenesis by acting upstream of Microprocessor activity in vivo.

Microprocessor cleavage activity was also substantially inhibited by CHR2(E1747A) that was pre-incubated with pri-miRNAs, but to a lesser extent than by CHR2 (Fig. 3c, Extended Data Fig. 5g). This result indicates that CHR2-mediated inhibition of Microprocessor activity in vitro results from features other than its SE-binding ability. By contrast, addition of CHR2(E1747A) to pri-miRNAs that had been pre-incubated with SE had only a marginal effect on miRNA production (Fig. 3d, Extended Data Fig. 5h). Thus, if SE binds to pri-miRNA before CHR2, obstruction of the CHR2–SE interaction compromises CHR2-mediated inhibition of pri-miRNA processing in vitro. Notably,

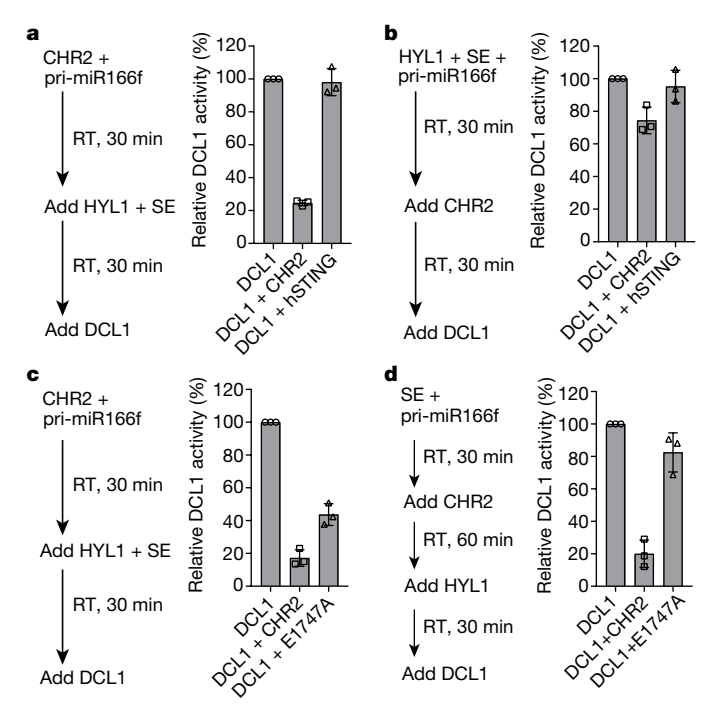


Fig. 3 | In vitro Microprocessor assays show that CHR2 inhibits pri-miRNA processing. a, Pre-incubation of CHR2 with pri-miRNAs inhibited pri-miRNA processing. b, Pre-incubation of HYL1–SE with pri-miRNAs largely bypassed the CHR2-mediated inhibition of pri-miRNA processing. c, Pre-incubation of pri-miRNA with CHR2(E1747A) substantially reduced pri-miRNA processing. d, CHR2(E1747A) marginally inhibited pri-miRNA processing when pri-miRNA was pre-incubated with SE. Molar ratio of SE:CHR2 (or CHR2(E1747A)) was 4:1. a–d, Left, reconstitution orders; right, quantification of relative cleavage efficiency with s.d. from three replicates.

these results are consistent with the observation that CHR2 requires SE to inhibit miRNA accumulation in vivo (Fig. 2c). Thus, we conclude that CHR2 obtains pri-miRNAs from SE to fulfil its inhibition of pri-miRNA processing.

CHR2 binds to pri-miRNAs

CHR2 does not block access of DCL1–HYL1 to SE to process pri-miR-NAs (Model 1, Extended Data Figs. 6, 7, Supplementary Information). Next, we asked whether CHR2 sequestered pri-miRNAs from SE, thwarting their handover to DCL1–HYL1 (Model 2, Extended Data Fig. 6a). Electrophoretic mobility shift assays (EMSAs) showed that CHR2 bound to pri-miRNAs and pre-miRNAs (apparent dissociation constant (K_d) = 18.78 \pm 0.70 nM; Hill coefficient (n_H) = 3.87) as strongly as to double-stranded DNA (dsDNA) (apparent $K_d \approx 16$ nM, n_H = 4.27) (Fig. 4a, Extended Data Fig. 8a–f). The sigmoidal CHR2–nucleic acid binding curve (Fig. 4a, Extended Data Fig. 8f) suggests cooperativity between multiple nucleic acid binding sites in CHR2²⁴ in substrate binding.

SE and HYL1 can also bind to pri-miRNAs^{18–20} with binding affinities of approximately 50 and 0.7 nM, respectively (Fig. 4b, Extended Data Fig. 8g, h). These results indicate that CHR2 binds to pri-miRNAs with a higher affinity than SE but with a substantially lower affinity than HYL1. The results also suggest that CHR2 has the potential to compete with SE, but not with HYL1, for pri-miRNAs. However, EMSA showed that co-incubation of CHR2 and SE with pri-miRNAs resulted in a shifting pattern different from the mobility of either CHR2-pri-miRNA or SE-pri-miRNA complexes (Fig. 4c). These results suggest that CHR2, SE, and pri-miRNA can form stable complexes with a distinct electrophoretic mobility. Alternatively, CHR2 may alter the pri-miRNA structure and thus, the mobility of the SE-pri-miRNA complex. By contrast, whenever HYL1 was applied, individually or combined with other proteins, the mobility of the pri-miRNA-protein complexes

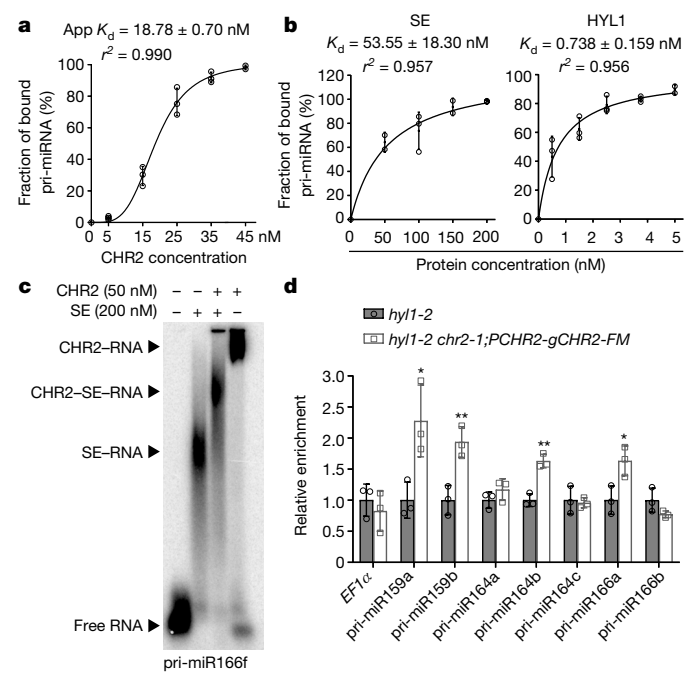


Fig. 4 | **CHR2 binds to pri-miRNAs in vitro and in vivo. a, b,** The binding curves of CHR2 (**a**), SE and HYL1 (**b**) to pri-miRNA. The (apparent) K_d values were calculated from the EMSA image quantification with s.d. from three experiments. **c,** EMSA shows that CHR2, SE and pri-miRNA form a ribonucleoprotein complex. **d,** RIP assay shows that CHR2 binds to pri-miRNAs in vivo. The relative signal of pri-miRNAs was calculated with s.d. from three biological repeats (*P < 0.05; **P < 0.01; unpaired, two-tailed Student's t-test).

was always identical to that of HYL1-pri-miRNA alone (Extended Data Fig. 8i). This result suggests that HYL1 could readily sequester pri-miRNAs from SE and/or CHR2 in vitro, and that CHR2 and SE could not preclude pri-miRNA handover to DCL1-HYL1 for processing. This result is also consistent with the observation that inhibition of Microprocessor activity by CHR2 can be largely attenuated when pri-miRNAs are pre-incubated with HYL1-SE (Fig. 3b).

Next, we performed ribonucleoprotein immunoprecipitation (RIP) experiments using *hyl1-2 chr2-1;PCHR2-gCHR2-FM* homozygotes containing unprocessed pri-miRNAs (Extended Data Fig. 8j). The RIP results showed that pri-miR159a, pri-miR159b, pri-miR164b, and pri-miR166a, which are the main contributors to their respective mature miRNAs, were all significantly enriched in the CHR2 immunoprecipitate, whereas this pattern was not observed for other pri-miRNAs (pri-miR164a and pri-miR164c) that do not contribute substantially to mature miRNAs (Fig. 4d). Moreover, treatment of the samples with RNases before reverse transcription did not yield any signals, suggesting that the enrichment was specifically from CHR2-bound RNAs (Extended Data Fig. 8k). Together, these results validated the theory that CHR2 binds to many species of nascent pri-miRNAs in vivo, further suggesting that CHR2 acts on SE-bound pri-miRNAs before their handover to DCL1–HYL1 in vivo.

CHR2 remodels SE-bound pri-miRNAs

Plants containing the hypomorphic *chr2-1a* allele with compromised ATPase activity retained enhanced miRNA accumulation compared to Col-0 plants (Extended Data Fig. 2d–g). Thus, inhibition of miRNA accumulation by CHR2 involves its ATPase activity. We next hypothesized that CHR2 might unwind self-complementary pri-miRNAs and alter their hairpin structures (Model 3, Extended Data Fig. 6a). To test this hypothesis, we conducted CHR2 remodelling assays with ³²P-labelled but nicked pri-miR166f. CHR2, but not HYL1, clearly released a large portion of the 26-nucleotide (nt) RNA fragment from the nicked pri-miR166f (Fig. 5a, Extended Data Fig. 9a–d). Therefore,

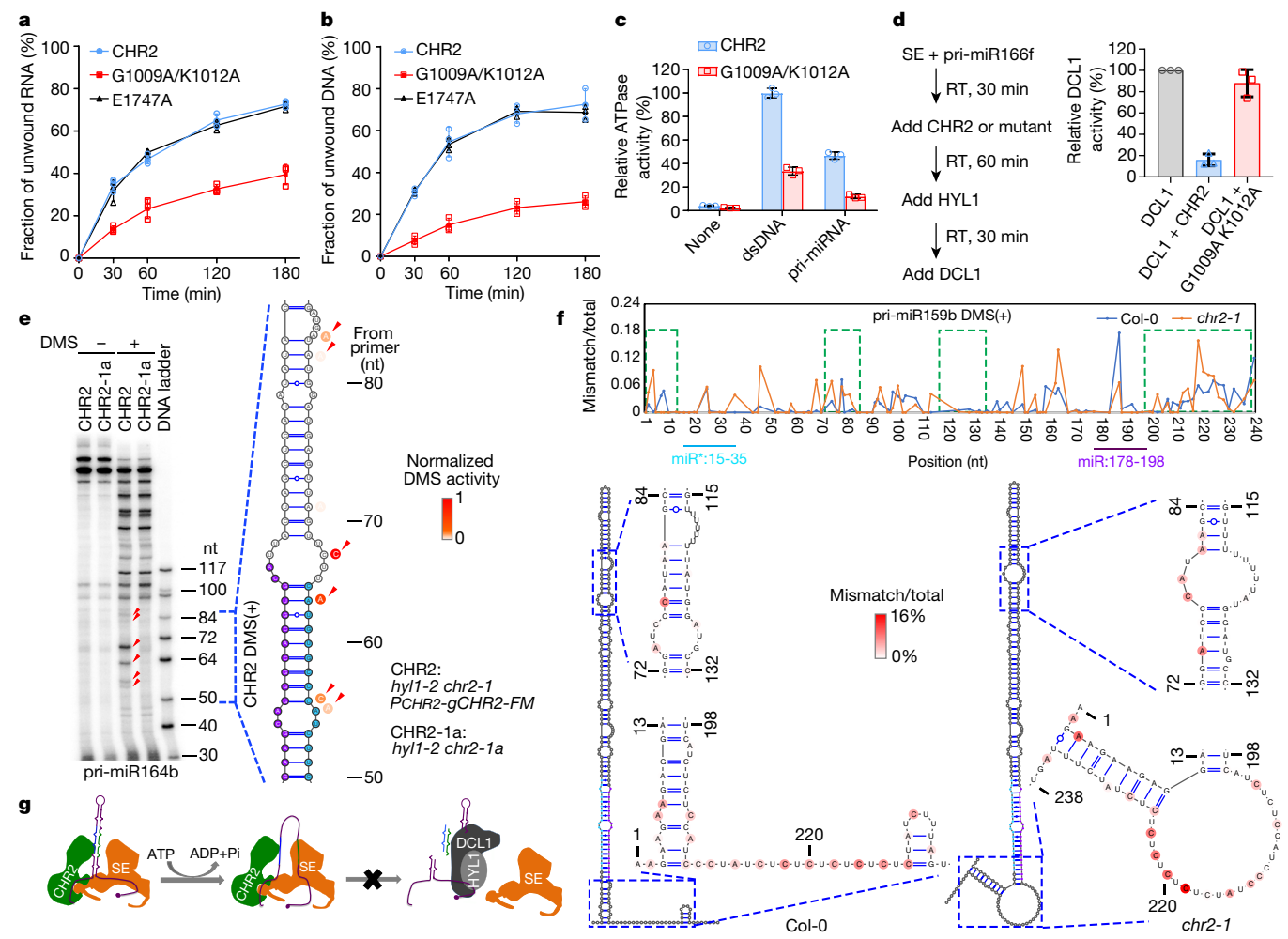


Fig. 5 | CHR2 remodels pri-miRNAs to prevent their processing. a, b, Time-course of remodelling and helicase activities of CHR2 and variants on pri-miRNAs (a) and dsDNA (b). c, Thin layer chromatography (TLC) assays shows ATPase activities of CHR2 and CHR2(G1009A/K1012A) with or without dsDNA or pri-miRNA. d, Right, Microprocessor assay shows that CHR2(G1009A/K1012A) did not inhibit pri-miRNA processing (right). Left, reconstitution order. In a-d, image quantifications were calculated with s.d. from three replicates. e, DMS-primer extension assays show nucleotides (red arrows) in pri-miR164b with stronger DMS

activities in *hyl1-2 chr2-1;PCHR2-gCHR2-FM* plants than in *hyl1-2 chr2-1a* plants. f, DMS–MaPseq analysis shows that CHR2 alters nucleotide pairings in upper stem and base region of pri-miR159b. Top, average mutation frequencies of A and C are plotted along pri-miRNA sequence. The regions within green dashed boxes correspond to zoomed-in secondary structures modelled from the DMS activities (bottom). Colour-coded nucleotides had different DMS activities between Col-0 and *chr2-1* plants. miRNA and * strands are shown in purple and cyan, respectively. g, Proposed model for inhibition of pri-miRNA processing by CHR2.

CHR2 does unwind pri-miRNAs, in a way similar to dsDNA (Fig. 5b, Extended Data Fig. 9e, f). These results were unexpected, as SWI/SNF complexes are mainly thought to lack helicase activity^{1,25}.

Similar to other SWI2/SNF2 ATPases^{26,27}, CHR2 had only basal ATPase activity in the ground state. Nonetheless, dsDNA and pri-miRNA stimulated its ATPase activity by approximately 25-fold and 12-fold, respectively (Fig. 5c, Extended Data Fig. 9g-i). The lower stimulation of ATPase activity by pri-miRNA relative to dsDNA was probably because it harbours mispairings and internal loops. Notably, mutations in the CHR2 ATP-binding site (G1009A/K1012A or N1392A/R1417A) diminished the dsDNA- and/or pri-miRNAstimulating ATPase activities of CHR2 by threefold (Fig. 5c, Extended Data Fig. 2e, 9g-i). Consistently, CHR2(G1009A/K1012A) and the CHR2 nucleotide-binding mutant (CHR2(D1355A/R1385A)), but not CHR2(E1747A), also strongly reduced the CHR2 remodelling/helicase activity (Fig. 5a, b, Extended Data Fig. 9c-f). These results indicate that the unwinding of dsDNA and pri-miRNAs by CHR2 is driven by ATP hydrolysis. In addition, the CHR2 mutants with alterations in the ATPand nucleotide-binding sites, but not the E1747A mutant, had slightly reduced affinity for pri-miRNAs relative to wild-type CHR2 (Extended Data Fig. 10a). Thus, the pri-miRNA binding and remodelling activities

of CHR2 depend on its ATPase domain, but not on the SE interaction interface.

We further performed Microprocessor assays using the remodelling-defective CHR2(G1009A/K1012A). As CHR2 is likely to access pri-miRNAs through SE in vivo (Fig. 2c), we pre-incubated SE protein with pri-miRNAs before the application of CHR2 or CHR2(G1009A/K1012A). Whereas CHR2 substantially inhibited Microprocessor activity, CHR2(G1009A/K1012A) had negligible effects on pri-miRNA processing (Fig. 5d, Extended Data Fig. 10b). The loss of inhibition of pri-miRNA processing was probably not caused by the slightly reduced affinity of CHR2(G1009A/K1012A) for pri-miRNAs compared to wild-type CHR2 (apparent $K_d \approx 19$ nM and 28 nM, respectively) because CHR2 and SE are in the same complex with pri-miRNAs (Fig. 4c). Rather, the result indicates that the CHR2 remodelling activity is critical for inhibition of pri-miRNA processing in vitro.

To study how the remodelling mutations affect miRNA accumulation in vivo, we created *chr2-1;PCHR2-gCHR2(G1009A/K1012A)-FM* and *chr2-1;PCHR2-gCHR2(D1355A/R1385A)-FM* transgenic lines. Notably, the morphological and miRNA accumulation defects seen in *chr2-1* plants were partially rescued in these transgenic plants (Extended Data Fig. 10c–e). We also introduced the *PMIR159b-FM-GUS* transgene into

the *chr2-1;PCHR2-gCHR2(G1009A/K1012A)-FM* hypomorphic line by crossing. Notably, the CHR2 variant reduced MIR gene transcription in *chr2-1;PCHR2-gCHR2(G1009A/K1012A)-FM;PMIR159b-FM-GUS* homozygotes (Extended Data Fig. 10f). Thus, the increase in miRNA abundance in the partial complementation lines should result from compromised post-transcriptional inhibition of pri-miRNA processing by CHR2 variants that lack the remodelling function.

CHR2 alters pri-miRNA folding in vivo

To determine whether CHR2 remodels pri-miRNAs in vivo, we probed RNA secondary structures through a dimethyl sulfide (DMS)-based method²⁸ (Extended Data Fig. 11a–c). DMS methylates the base-pairing faces of adenosine (A) and cytidine (C) of RNA in loops, bulges, mismatches and joining regions, and such methylation precludes the reverse transcription reaction. Strikingly, the reactivity of DMS with pri-miR164b differed between transgenic plants expressing wild-type CHR2 and those expressing CHR2-1a, which has defective ATPase activity (Fig. 5e, Extended Data Fig. 2d–g, 11d). Enhanced DMS modifications, detected by premature termination of reverse transcription, were observed in the miRNA/* duplex and the proximal upper stem of pri-miR164b in CHR2 plants compared to *chr2-1a* plants. This result indicates that there are more unpaired or unprotected nucleotides in the duplex region of pri-miR164b in a CHR2 background than in the *chr2* mutant.

Finally, we adopted a method of DMS mutational profiling with Illumina sequencing (DMS-MaPseq) to target multiple RNAs in vivo²⁹ (Extended Data Fig. 11a). DMS-MaPseq uses a special reverse transcriptase enzyme from a group II self-splicing intron (TGIRT)³⁰. TGIRT can read through the DMS-modified A and C template bases and insert mismatches into the corresponding cDNAs, thereby providing signatures for mapping of DMS modifications along reverse transcription products²⁹. We targeted 16 pri-miRNAs, and eight were successfully and consistently amplified between two biological replicates. Notably, DMS-MaPseq showed meaningful differences in DMS reactivity of the eight pri-miRNAs, but not the control UBQ4 mRNA, between Col-0 and *chr2-1* plants (Fig. 5f, Extended Data Fig. 11e-h, 12). First, pri-miR166a and pri-miR168a tended to form shortened upper stems and branched terminal loops in Col-0 plants, whereas they displayed extended upper stems and linear terminal loops in *chr2-1* plants (Extended Data Fig. 11g, h). As multi-branched terminal loops and shortened upper stems can cause loop-to-base abortive processing of pri-miRNAs whereas elongated upper stems promote productive processing of pri-miRNAs¹², CHR2 might remodel the structures of terminal loops and upper stems to control the productive processing of pri-miRNAs. Second, modelling of pri-miR168b folding showed that the lower stem was increased from 9 nt in Col-0 plants to 16 nt in *chr2-1* plants (Extended Data Fig. 12a). Such an increase places miR168b/* an ideal distance of 15–17 nt from a reference single-strand basal loop region¹², allowing accurate processing of pri-miR168b. Finally, primiR159 and pri-miR319 are sequentially processed from terminal loop to base to eventually release miRNA/*31. In chr2-1 plants, pri-miR159b and pri-miR319b had stronger DMS reactivity in the upper stems, suggesting lesser folding or more unpaired nucleotides in these regions and potentially increasing pri-miRNA processing from the terminal loop to the lower base (Fig. 5f; Extended Data Fig. 12b). Furthermore, the lower stem of pri-miR159b was also altered so that miR159/* was immediately adjacent to a bigger and more basal loop in *chr2-1* plants (Fig. 5f). This conformation is likely to further promote accurate and efficient processing of miRNA/* from pre-miRNAs, as both animal Dicer and plant DCL1 recognize the loop-bulge structures in addition to the 5' and 3' ends of pre-miRNAs for accurate processing 12,32. Thus, CHR2 alters the in vivo secondary structures of pri-miRNAs or, possibly, their association with cellular components in various ways.

Discussion

Here we report a non-canonical function of CHR2 in miRNA biogenesis: while CHR2 positively regulates transcription of MIR loci owing

to its conventional chromatin remodelling activity, it can also directly inhibit post-transcriptional processing of pri-miRNAs. On the basis of our results, we propose a model in which CHR2 inhibits miRNA production by obtaining pri-miRNAs from SE and remodelling the RNA substrates, rendering them unsuitable for processing by Microprocessor (Fig. 5g). Thus, the SWI2/SNF2 ATPase goes beyond its canonical substrates of nucleosome¹ and Polycomb complexes³³, and acts directly on its new substrate of pri-miRNAs. The biological significance of these self-opposing functions in miRNA biogenesis is that CHR2 provides a new and balanced regulatory mechanism to stabilize the supply of proper substrates upstream of Microprocessor activity. In this scenario, CHR2-SE may serve as a specific reader and modifier of sequences and structures of pri-miRNAs and fine-tune miRNA biogenesis in vivo. This mechanism may also partially explain frequently observed inconsistencies between the expression of MIR genes and the abundance of mature miRNAs^{14,15}.

Several cellular components, including transcription factors, can increase or decrease Microprocessor activity by modulating or sequestering core or regulatory Microprocessor components ^{34–37}. However, CHR2 can act as both a positive and a negative regulator of miRNA biogenesis, and the net outcome depends on the balance of two opposite forces. Thus, CHR2 represents a new paradigm for the regulation of miRNA biogenesis by exerting opposing effects in consecutive biological processes (pri-miRNA transcription and processing) through the conformation of different protein complexes (SWI/SNF and CHR2–SE), acting on different molecular substrates (chromatin and structured RNA, respectively). As CHR2 and SE/Ars2 are conserved throughout eukaryotes, it would be interesting to learn whether such a mechanism exists beyond *Arabidopsis*. Moreover, whether CHR2 and SE/Ars2 participate in remodelling of pre-mRNPs and lncRNA complexes besides pri-miRNAs would also be an exciting topic for future investigation.

Online content

Any Methods, including any statements of data availability and Nature Research reporting summaries, along with any additional references and Source Data files, are available in the online version of the paper at https://doi.org/10.1038/s41586-018-0135-x

Received: 21 September 2017; Accepted: 9 March 2018; Published online: 16 May 2018

- Clapier, C. R., Iwasa, J., Cairns, B. R. & Peterson, C. L. Mechanisms of action and regulation of ATP-dependent chromatin-remodelling complexes. *Nat. Rev. Mol. Cell Biol.* 18, 407–422 (2017).
- Batsché, E., Yaniv, M. & Muchardt, C. The human SWI/SNF subunit Brm is a regulator of alternative splicing. Nat. Struct. Mol. Biol. 13, 22–29 (2006).
- Tyagi, A., Ryme, J., Brodin, D., Ostlund Farrants, A. K. & Visa, N. SWI/SNF associates with nascent pre-mRNPs and regulates alternative pre-mRNA processing. PLoS Genet. 5, e1000470 (2009).
- Babour, A. et al. The chromatin remodeler ISW1 is a quality control factor that surveys nuclear mRNP biogenesis. Cell 167, 1201–1214.e15 (2016).
- Kawaguchi, T. et al. SWI/SNF chromatin-remodeling complexes function in noncoding RNA-dependent assembly of nuclear bodies. *Proc. Natl Acad. Sci.* USA 112, 4304–4309 (2015).
- 6. Han, P. et al. A long noncoding RNA protects the heart from pathological hypertrophy. *Nature* **514**, 102–106 (2014).
- Zhu, P. et al. LncBRM initiates YAP1 signalling activation to drive self-renewal of liver cancer stem cells. Nat. Commun. 7, 13608 (2016).
- Prensner, J. R. et al. The long noncoding RNA SChLAP1 promotes aggressive prostate cancer and antagonizes the SWI/SNF complex. *Nat. Genet.* 45, 1392–1398 (2013).
- Li, S., Castillo-González, C., Yu, B. & Zhang, X. The functions of plant small RNAs in development and in stress responses. *Plant J.* 90, 654–670 (2017).
- Nguyen, T. A. et al. Functional anatomy of the human Microprocessor. Cell 161, 1374–1387 (2015).
- Ha, M. & Kim, V. N. Regulation of microRNA biogenesis. Nat. Rev. Mol. Cell Biol. 15, 509–524 (2014).
- Zhu, H. et al. Bidirectional processing of pri-miRNAs with branched terminal loops by Arabidopsis Dicer-like1. Nat. Struct. Mol. Biol. 20, 1106–1115 (2013).
- Rogers, K. & Chen, X. Biogenesis, turnover, and mode of action of plant microRNAs. Plant Cell 25, 2383–2399 (2013).
- 14. Barciszewska-Pacak, M. et al. *Arabidopsis* microRNA expression regulation in a wide range of abiotic stress responses. *Front. Plant Sci.* **6**, 410 (2015).
- Thomson, J. M. et al. Extensive post-transcriptional regulation of microRNAs and its implications for cancer. Genes Dev. 20, 2202–2207 (2006).

RESEARCH ARTICLE

- Grigg, S. P., Canales, C., Hay, A. & Tsiantis, M. SERRATE coordinates shoot meristem function and leaf axial patterning in *Arabidopsis. Nature* 437, 1022–1026 (2005).
- Dong, Z., Han, M. H. & Fedoroff, N. The RNA-binding proteins HYL1 and SE promote accurate *in vitro* processing of pri-miRNA by DCL1. *Proc. Natl Acad. Sci.* USA 105, 9970–9975 (2008).
- Iwata, Y., Takahashi, M., Fedoroff, N. V. & Hamdan, S. M. Dissecting the interactions of SERRATE with RNA and DICER-LIKE 1 in *Arabidopsis* microRNA precursor processing. *Nucleic Acids Res.* 41, 9129–9140 (2013).
- Machida, S., Chen, H. Y. & Adam Yuan, Y. Molecular insignts into miRNA processing by *Arabidopsis* thaliana SERRATE. *Nucleic Acids Res.* 39, 7828–7836 (2011).
- Yang, S. W. et al. Structure of Arabidopsis HYPONASTIC LEAVES1 and its molecular implications for miRNA processing. Structure 18, 594–605 (2010).
- 21. Gruber, J. J. et al. Ars2 links the nuclear cap-binding complex to RNA interference and cell proliferation. *Cell* **138**, 328–339 (2009).
- Sabin, L. R. et al. Ars2 regulates both miRNA- and siRNA- dependent silencing and suppresses RNA virus infection in *Drosophila*. Cell 138, 340–351 (2009).
- Shu, C., Yi, G., Watts, T., Kao, C. C. & Li, P. Structure of STING bound to cyclic di-GMP reveals the mechanism of cyclic dinucleotide recognition by the immune system. *Nat. Struct. Mol. Biol.* 19, 722–724 (2012).
- Farrona, S., Hurtado, L. & Reyes, J. C. A nucleosome interaction module is required for normal function of *Arabidopsis thaliana* BRAHMA. *J. Mol. Biol.* 373, 240–250 (2007).
- 25. Côté, J., Qùinn, J., Workman, J. L. & Peterson, C. L. Stimulation of GAL4 derivative binding to nucleosomal DNA by the yeast SWI/SNF complex. *Science* **265**, 53–60 (1994).
- Liu, X., Li, M., Xia, X., Li, X. & Chen, Z. Mechanism of chromatin remodelling revealed by the Snf2-nucleosome structure. *Nature* 544, 440–445 (2017).
- Dürr, H., Körner, C., Müller, M., Hickmann, V. & Hopfner, K. P. X-ray structures of the Sulfolobus solfataricus SWI2/SNF2 ATPase core and its complex with DNA. Cell 121, 363–373 (2005).
- Ding, Y. et al. In vivo genome-wide profiling of RNA secondary structure reveals novel regulatory features. *Nature* 505, 696–700 (2014).
- 29. Zubradt, M. et al. DMS-MaPseq for genome-wide or targeted RNA structure probing *in vivo*. *Nat. Methods* **14**, 75–82 (2017).
- Mohr, S. et al. Thermostable group II intron reverse transcriptase fusion proteins and their use in cDNA synthesis and next-generation RNA sequencing. RNA 19, 958–970 (2013).
- Bologna, N. G., Mateos, J. L., Bresso, E. G. & Palatnik, J. F. A loop-to-base processing mechanism underlies the biogenesis of plant microRNAs miR319 and miR159. EMBO J. 28, 3646–3656 (2009).
- 32. Gu, S. et al. The loop position of shRNAs and pre-miRNAs is critical for the accuracy of dicer processing *in vivo*. *Cell* **151**, 900–911 (2012).

- 33. Kadoch, C. et al. Dynamics of BAF-Polycomb complex opposition on heterochromatin in normal and oncogenic states. *Nat. Genet.* **49**, 213–222 (2017).
- Davis, B. N., Hilyard, A. C., Lagna, G. & Hata, A. SMAD proteins control DROSHA-mediated microRNA maturation. *Nature* 454, 56–61 (2008)
- Suzuki, H. I. et al. Modulation of microRNA processing by p53. Nature 460, 529–533 (2009).
- Cheng, T. L. et al. MeCP2 suppresses nuclear microRNA processing and dendritic growth by regulating the DGCR8/Drosha complex. Dev. Cell 28, 547–560 (2014).
- Mori, M. et al. Hippo signaling regulates microprocessor and links cell-densitydependent miRNA biogenesis to cancer. Cell 156, 893–906 (2014).

Acknowledgements We thank A. Jerzmanowski and Y. Cui for sharing *CHR2* plasmids and *chr2-1* alleles; A. Millar for *PMIR159a-GUS* and *PMIR159b-GUS* lines; P. He and P. Manavella for Y3H constructs; C. Kaplan and T. Devarenne for reading the manuscript; R. Hays for technical advice; and L. Zeng and F. Raushel for equipment and facility support. This work was supported by the NSF grant MCB-1716243 and CPRIT grant RP160822 to X.Z. D.S. and Y.L. were supported by the China Scholar Council Fellowship.

Reviewer information *Nature* thanks K. P. Hopfner, Z. Szweykowska-Kulińska and P. Waterhouse for their contribution to the peer review of this work.

Author contributions X.Z. conceptualized the study. X.Z., Z.W. and C.C.-G. designed experiments. X.Z. performed gel filtration chromatography and immunoprecipitation with mass spectrometry. Z.W. performed all biochemistry assays, genetic and molecular studies, RIP, in vivo pri-miRNA structure probing, and part of the analysis of high-throughput sequencing data. Z.M. performed subcellular localization assays and analysed high-throughput sequencing data. C.C.-G. performed protein alignment and provided intellectual input. D.S. performed LCI assay. Y.L. performed part of the Y2H and Y3H and genotyping assays. B.Y. provided antibodies and additional reagents. B.Z. and P.L. provided the baculovirus/insect expression system and intellectual input. X.Z. and Z.W. wrote the manuscript.

Competing interests The authors declare no competing interests.

Additional information

Extended data is available for this paper at https://doi.org/10.1038/s41586-018-0135-x.

Supplementary information is available for this paper at https://doi.org/10.1038/s41586-018-0135-x.

Reprints and permissions information is available at http://www.nature.com/reprints.

Correspondence and requests for materials should be addressed to X.Z. **Publisher's note:** Springer Nature remains neutral with regard to jurisdictional claims in published maps and institutional affiliations.

METHODS

Plant materials and growth conditions. *Arabidopsis thaliana* ecotype Columbia (Col-0), *chr2-1* (SALK_030046), *se-1* (CS3257), *se-2* (SAIL_44_G12), *se-3* (SALK_083196), *hyl1-2* (SALK_064863) and *dcl1-9* (CS3828) were used for this study.

For generating complementation and point mutation (partial complementation) lines, the heterozygous $chr2\cdot 1^{+/-}$ mutant was transformed with binary vectors of PCHR2-gCHR2-FM or its derivatives by the floral dip transformation method³⁸. In T2 transgenic plants, the homozygous $chr2\cdot 1$ background was genotyped by PCR using specific primers (Supplementary Table 4); transgenic plants harbouring dual-tagged CHR2 and its derivatives were screened by western blot analysis. The pleiotropic phenotype of $chr2\cdot 1$ was fully rescued in the T2 progeny of the $PCHR2\cdot gCHR2\cdot FM$ transgenic plants, indicating that dual-tagged CHR2 is as functionally active as wild-type CHR2.

Double mutants such as *chr2-1a se-3*, *chr2-1a hyl1-2* and *chr2-1a dcl1-9* were obtained by crossing the partial complementation line of *chr2-1;PCHR2-gCHR2(N1392A/R1417A)-FM* #49 (termed *chr2-1a*) with heterozygous *se-3*, homozygous *hyl1-2* and heterozygous *dcl1-9* lines respectively. In the F2 generation, homozygous double mutants were identified by PCR using primers listed in Supplementary Table 4.

The *hyl1-2 chr2-1;PCHR2-gCHR2-FM* material was obtained by crossing the complementation line of *chr2-1;PCHR2-gCHR2-FM* #8 with *hyl1-2* plants. In the F2 generation, homozygous *hyl1-2 chr2-1;PCHR2-gCHR2-FM* plants were identified by PCR using primers listed in Supplementary Table 4.

For GUS histochemical analysis, heterozygous *chr2-1*^{+/-} plants were transformed with the MIR promoter-driven *FM-GUS* (PMIR159a-FM-GUS, PMIR159b-FM-GUS, PMIR164b-FM-GUS and PMIR164c-FM-GUS vectors) by floral transformation³⁸. In T2 transgenic plants, homozygous *chr2-1*^{-/-} plants were identified by phenotypic segregation. *chr2-1;PCHR2-gCHR2(E1747A)-FM;PMIR159a-FM-GUS* and *chr2-1;PCHR2-gCHR2(G1009A/K1012A)-FM;PMIR159b-FM-GUS* plants were obtained by crossing *chr2-1*^{+/-};*PCHR2-gCHR2(E1747A)-FM* #7 and *chr2-1;PCHR2-gCHR2(G1009A/K1012A)-FM* #7 lines with *chr2-1*^{+/-};*PMIR159a-FM-GUS* #3 and *chr2-1*^{+/-};*PMIR159b-FM-GUS* #5 lines, respectively. In the F2 generations, homozygous double mutants were identified by PCR using primers listed in Supplementary Table 4.

Plants were grown as previously described³⁹. Wild-type (Col-0), mutants and transgenic lines were grown under a 12 h light–12 h dark cycle. Typically, three-week-old plants were harvested for various assays including picture-taking, sRNA blot and western blot analyses unless specifically mentioned. No statistical methods were used to predetermine sample size. Randomizations and blinding design were not relevant to this study.

Vector construction. Most coding DNA sequences (CDSs) and genomic sequences were cloned into pENTR/D-TOPO (Thermo Fisher) vectors and confirmed by sequencing. The majority of plant binary constructs were made using the Gateway system (Thermo Fisher). The primers for all constructs are listed in Supplementary Table 4.

PCHR2-gCHR2-FM-3'UTR and its derivatives were constructed as follows: first, three truncations of CHR2 genomic fragment were amplified and cloned into pENTR/D vectors to generate pENTR-gCHR2-Truncation1-3; then, pEN-TR-gCHR2-Truncation1 and 2 were digested with XhoI/AscI and ligated to create pENTR/D-gCHR2-Truncation1+2; later, pENTR-gCHR2-Truncation1+2 and Truncation 3 were digested with BamHI/AscI, and ligated to create pENTR/DgCHR2. Second, a fragment of Flag-4Myc (FM) was amplified and inserted 3' of the DC cassette in a pBA002a-FM-DC vector¹² to generate pBA002a-FM-DC-FM. Subsequently, the 3' UTR of CHR2 (493 bp) was amplified and cloned into the SpeI/SacI-digested pBA002a-FM-DC-FM vector to yield pBA002a-FM-DC-FM-3'UTR. In parallel, the promoter of CHR2 (1,903 bp) was amplified and cloned into the XbaI/EcoRV-digested pBA002a-FM-DC to yield pBA002a-PCHR2-FM-DC. The resultant pBA002a-PCHR2-FM-DC vector was digested with ApaI/XbaI and ligated to the same enzyme-treated pBA002a-FM-DC-FM-3'UTR to produce pBA002a-PCHR2-FM-DC-FM-3'UTR. The plasmid was digested with XbaI/AscI to remove the FM tag in front of the DC cassette, blunted by Klenow treatment, and self-ligated to create the pBA002a-PCHR2-DC-FM-3'UTR vector. Finally, the full length of the CHR2 genomic fragment from a pENTR vector was transferred into pBA002a- PCHR2-DC-FM-3'UTR by Gateway attL-attR (LR) recombination reaction (ThermoFisher) to yield pBA002a-PCHR2-gCHR2-FM-3'UTR.

Site-specific mutations were introduced into *CHR2* by PCR using pEN-TR-gCHR2 truncations as templates. Then the fragments containing point mutations were swapped into pENTR-gCHR2 using restriction enzyme digestion followed by ligation. Finally, the *CHR2* genomic fragment containing site-specific point mutations was transferred into pBA002a-PCHR2-DC-FM-3'UTR by LR reaction to yield pBA002a-PCHR2-gCHR2 mutants-FM-3'UTR.

PMIR-FM-GUS were constructed as follows: First, approximately 1.8–2.4-kb promoters of MIR159a, MIR159b, MIR164a, MIR164b and MIR164c were amplified

using pairs of primers listed in Supplementary Table 4, and cloned into pENTR/D vectors. Second, pBA002a-FM-DC-FM (as above) was treated with XbaI/AscI to remove the FM tag in front of the DC cassette, blunted by Klenow treatment, and self-ligated to produce the pBA002a-DC-FM vector; then, *GUS* CDS was amplified from pBA-GUS and cloned into the XhoI/PacI-digested pBA002a-DC-FM to create pBA002a-DC-FM-GUS. Finally, the promoters of MIR genes were transferred into pBA002a-DC-FM-GUS to yield PMIR-FM-GUS vectors.

P35S-FM-SE and PSE-FM-SE were constructed as follows: For P35S-FM-SE, *SE* CDS was transferred into pBA-FM-DC¹² by LR reaction to yield he P35S-FM-SE construct. For PSE-FM-SE, the *SE* promoter (2,241 bp) was amplified and cloned into BamHI/XbaI-digested pBA002a-FM-DC to yield pBA002a-PSE-FM-DC. Then the *SE* CDS was transferred into pBA002a- PSE-FM-DC by LR reaction to yield PSE-FM-SE vectors.

P35S-CHR2-YFP and P35S-SE-CFP were constructed as follows: For P35S-CHR2-YFP, first, two truncations of *CHR2* CDS were amplified and cloned into pCR-BluntII-TOPO vectors. Next, NotI/NdeI-digested *CHR2* truncation 1 and NdeI/AscI-digested *CHR2* truncation 2 were ligated into NotI/AscI-digested pEN-TR/D to yield pENTR/D-CHR2. Then, *CHR2* CDS was transferred into pBA-DC-YFP by LR reaction to create a P35S-CHR2-YFP vector. For P35S-SE-CFP, the *SE* CDS was transferred into pBA-DC-CFP by LR reaction to create P35S-SE-CFP vectors

GST-CHR2-957-1823aa-6×His and its variants were constructed as follow: CHR2-957-1823aa-6×His and its derivatives were amplified from pENTR-CHR2 and pENTR-CHR2 mutants using sets of primers: 5' forward containing an EcoRI digesting site and 3' reverse primer containing 6×His tag sequence and Sall digestion site, respectively (Supplementary Table 4). Then the PCR products were cloned into an EcoRI/SalI-digested pGEX-4T-1 vector to produce pGEX-4T-1-GST-CHR2-957-1823aa derivatives-6×His.

GST-6×His-DCL1, 6×His-SUMO-HYL1 and 6×His-SUMO-SE were constructed as follows: For the GST-6×His-DCL1 construct, pBA002a-Flag-DCL1 was digested with XbaI/SpeI and blunted with Klenow treatment. Next, the *Flag-DCL1* blunt fragment was ligated into Smal-digested pAcGHLT-C (BD Biosciences) to yield the pAcGHLT-GST-6×His-DCL1 construct. For the 6×His-SUMO-SE construct, *SE* CDS was amplified and ligated into a BamHI/XbaI-digested pET28a-Avi-6×His-SUMO vector⁴⁰ to obtain the pET28a-Avi-6×His-SUMO-SE construct. For the 6×His-SUMO-HYL1 construct, *HYL1* CDS was amplified from the pBA-Myc-HYL1 plasmid¹² and digested with BamHI/SacI. The resultant fragment was ligated into the BamHI/SacI-treated pET28a-6×His-SUMO vector⁴⁰ to produce the pET28a-6×His-SUMO-HYL1 construct.

Yeast-two-hybrid (Y2H) and three-hybrid (Y3H) vectors were constructed as follows: For Y2H vectors, full-length and truncation derivatives of *SE*, *DCL1*, *HYL1* and *CHR2* or *CHR2* variants were cloned into vectors of pGADT7-GW, which harbours a GAL4 activation domain (AD), and pGBKT7-GW, which harbours a DNA binding domain (BD), using the LR reaction. Similarly, full-length *AtPrp40b* CDS was amplified and cloned into a pENTR/D-TOPO vector and confirmed by sequencing. Then the *AtPrp40b* CDS was cloned into a pGADT7-GW vector using the LR reaction. For Y3H vectors, a synthesized DNA fragment containing NotI, KpnI, SpeI, NcoI, AscI and BgIII digestion sites was digested by NotI and BgIII and cloned into a NotI/BgIII-digested pBridge (Clontech) vector to produce pBridge-MCSII. Then the *SE* CDS amplified from pENTR/D-SE was cloned into the pBridge-MCSII vector by EcoRI/BamHI to yield pBridge-BD-SE-MCSII. Finally, the *CHR2* CDS fragment was obtained from pENTR-CHR2 using NotI/AcsI digestion and cloned into the NotI/AscI-digested pBridge-BD-SE-MCSII to producing the pBridge-BD-SE-CHR2 vector.

Gel filtration chromatography of protein extracts from plants. Nine-day-old $\it P35S\text{-}FM\text{-}SE$ seedlings were harvested and homogenized in extraction buffer (20 mM Tris-HCl pH7.5, 150 mM NaCl, 4 mM MgCl $_2$, 75 μ M ZnCl $_2$, 1% glycerol, 1 pellet per 12.5 ml Complete EDTA-free protease inhibitor (Roche), 1 mM PMSF, and 15 μ M MG132). The homogenates were centrifuged twice at 15,000 r.p.m. for 15 min at 4 °C, and the final supernatant was filtered through a 0.2- μ m filter. Next, the total protein extracts were injected into an AKTA FPLC system, and the proteins were fractioned through a Superdex 200 10/300 GL column (GE Healthcare). Fractions were collected for western blot analysis of FM-SE protein. The Superdex 200 column was also calibrated by gel filtration standard (Bio-Rad).

Immunoprecipitation and mass spectrometry. In brief, nine-day-old wild-type and *P35S-FM-SE* transgenic seedlings were harvested and ground in liquid nitrogen. Total proteins were extracted from 10 g ground powder in 40 ml immunoprecipitation buffer (20 mM Tris-HCl pH 7.5, 150 mM NaCl, 4 mM MgCl₂, 75 µM ZnCl₂, 1% glycerol, 1 pellet per 12.5 ml Complete EDTA-free protease inhibitor (Roche), 1 mM PMSF, and 15 µM MG132). After being cleared by ultracentrifugation, the protein complexes were immunoprecipitated using anti-FLAG M2 magnetic beads (Sigma, Cat#: M8823) at 4°C for 2 h. After incubation, anti-FLAG M2 magnetic beads were washed four times with immunoprecipitation buffer for

5 min each at 4 °C, and protein complexes were then eluted by competitive $3\times$ Flag peptide (100 µg/ml). The recovered protein complexes were re-suspended in the immunoprecipitation buffer and subsequently immunoprecipitated with anti-c-Myc-agarose affinity gel (Sigma, Cat#: A7470) at 4 °C for 1.5 h. Next, the beads were washed four times with immunoprecipitation buffer to remove unspecific-bound proteins. Finally, the protein complexes were eluted in elution buffer (5 mM EDTA, 200 mM NH₄OH) for mass spectrometry analysis in the Taplin Mass Spectrometry Facility at Harvard Medical School.

Y2H and Y3H assays. The Matchmaker Gold Y2H system (Clontech) was used for Y2H assays. The constructs were co-transformed into the Y2H Gold yeast strain (Clontech) and selected on medium lacking leucine, tryptophan, histidine and adenine for Y2H assays. The pBridge construct (Clontech) was used for Y3H assays. The constructs were co-transformed into the Y2H Gold yeast strain (Clontech) and selected on medium lacking leucine, tryptophan, histidine and methionine but supplemented with 5 mM 3-amino-1,2,4-triazole (3-AT) for Y3H assays. For both Y2H and Y3H assays, positive colonies were picked up and dropped on the selective plates with 1:5 (for Y2H) or 1:10 (for Y3H) serial dilutions for the picture recording. Co-immunoprecipitation. Three-week-old plants on soil were sampled and ground in liquid nitrogen. Total proteins were extracted from 1 g ground powder in 5 ml immunoprecipitation buffer (40 mM Tris-HCl pH 7.5, 50 mM KCl, 5 mM MgCl₂, 5 mM DTT, 0.2 mM EDTA, 0.2% Triton X-100, 2% glycerol, 1 mM PMSF, $25 \,\mu\text{M}$ MG132, 1 pellet per 10 ml Complete EDTA-free protease inhibitor (Roche)); then, protein extracts were immunoprecipitated with the anti-FLAG M2 magnetic bead at 4°C for 2 h; for RNase treatment, 250 µl RNase A (1 mg/ml) was added to 5 ml immunoprecipitation buffer during incubation. After incubation, the beads were washed four times with immunoprecipitation buffer at 4°C for 5 min before application of SDS loading buffer at 95 °C for 10 min.

Confocal microscopy. Protoplast preparation and transfection were performed as described⁴¹. Transfected *Arabidopsis thaliana* protoplasts were imaged on an Olympus FV1000 confocal microscope.

Luciferase complementary imaging assay (LCI assay). The CDSs of *CHR2* and *SE* were cloned into *pCAMBIA-NLuc* and *pCAMBIA-CLuc*, respectively, by the LR reaction. Then the constructs were transformed into *A. tumefaciens* strain GV3101. LCI assays were performed as described⁴².

sRNA and western blot analyses. sRNA and western blot assays were performed as described³⁹. The sequences of the oligo probes for sRNA blot assays are listed in Supplementary Table 4. Western blot assays of CHR2-FM and its variants were typically conducted with an anti-Myc antibody throughout the study (Sigma, Cat#: C3956). Western blot assays of FM-GUS protein were performed with an anti-Flag antibody (Sigma, Cat#: F1804). Other endogenous protein-specific antibodies used in the study included anti-actin (Sigma, Cat#: A0480), anti-HYL1 (from B. Yu's laboratory), anti-DCL1 (from B. Yu's laboratory) and anti-SE (Agrisera, Cat#: AS09 532A). Secondary antibodies were goat-developed anti-rabbit and anti-mouse IgG (GE Healthcare, Cat#: NA934 and NA931).

sRNA sequencing and bioinformatics. Total RNA was prepared from three-week-old plants grown on soil using TRI Reagent (Sigma). Construction of sRNA libraries, Illumina sequencing and bioinformatic analysis were performed as described³⁹. Until now, 371 miRNAs have been annotated in *Arabidopsis*, and we initially calculated their expression levels (reads per million, RPM) based on total reads. This analysis revealed that 33 miRNAs were significantly over-accumulated in the *chr2-1* mutant. However, the RPM values of numerous miRNAs including the founding members (miR159 and miR166) did not match the results that were consistently obtained from sRNA blot analysis throughout our experiments. This observation suggested that high-throughput sequencing using standard barcodes might introduce a bias against many species of miRNAs as reported previously^{43,44}. To solve this issue, we normalized expression reads of miRNAs based on miR390, which consistently showed no changes between *chr2-1* and Col-0 plants in both sRNA blots and sRNA sequencing assays.

GUS histochemical analysis. Three-week-old transgenic plants were sampled and placed into a sodium phosphate solution containing 2 mM X-Gluc. The plants were vacuum infiltrated for 45 min and incubated at 37 °C overnight. After removal of chlorophyll, pictures of plants were taken with an Olympus SZH10 stereo microscope.

RNA extraction, reverse transcription, quantitative real-time PCR (RT-qPCR), and semiquantitative PCR. Total RNA was extracted from the three-week-old plants on soil using TRI Reagent (Sigma). cDNA synthesis, quantitative real-time PCR and semiquantitative PCR were performed as previously described³⁹. Primers are listed in Supplementary Table 4.

Alternative splicing analysis. Alternative splicing in $\it chr2-1$ was examined using rMATS software 45

Gene ontology analysis. Gene ontology analyses were performed with the agriGO toolkit⁴⁶.

Expression and purification of recombinant proteins. GST-6×His-DCL1 protein was expressed in a baculovirus/insect cell expression system, whereas

 $6\times$ His-SUMO-HYL1, $6\times$ His-SUMO-SE, GST-CHR2-957-1823aa- $6\times$ His and its derivatives were expressed in *Escherichia coil* BL21 (DE3) cells. All protein purification was performed at 4 °C, and purified proteins were finally frozen by liquid nitrogen and stored at $-80\,^{\circ}\text{C}$.

For expression and purification of DCL1, pAcGHLT-GST-6×His-DCL1 was co-transfected with BaculoGold baculovirus DNA (BD Biosciences, Cat # 554740) into sf9 insect cells (BD Biosciences Cat # 554738; authenticated by the vendor BD Biosciences) to generate recombinant baculovirus according to the manufacturer's instructions. The recombinant viruses were amplified for two rounds, and P3 virus was collected for large-scale protein expression. P3 virus was added to 2.5×10^6 sf9 insect cells per ml for propagation, and insect cells were collected 62 h later.

The DCL1 protein was purified by two-step affinity chromatography (Ni-NTA affinity and glutathione S-transferase affinity) followed by gel filtration chromatography. The cell pellet was re-suspended in lysis buffer (100 mM Tris-HCl pH 8.0, 300 mM KCl, 2% glycerol, 1 mM β -mercaptoethanol, 1 mM PMSF, 1% Triton X-100, 1 pellet per 50 ml Complete EDTA-free protease inhibitor (Roche)) and disrupted with a high pressure homogenizer (AVESTIN, Cat#: EF-C3). After centrifugation and filtration with 0.4-µm membrane, the cleared lysate was supplemented with 20 mM imidazole and loaded on a HisTrap HP column (GE Healthcare, Cat#: 17-5248-02). The column was washed with 25 ml wash buffer (40 mM Tris-HCl pH 8.0, 300 mM KCl, 2% glycerol, 1 mM β -mercaptoethanol, 1 mM PMSF, 80 mM imidazole) and eluted with gradient elution buffer from 80 to 150 mM imidazole (40 mM Tris-HCl pH 8.0, 300 mM KCl, 2% glycerol, 1 mM β-mercaptoethanol, 1 mM PMSF). The peak fractions containing recombinant GST-6×His-DCL1 proteins were pooled and dialysed with 2 litre GST dialysis buffer (40 mM Tris-HCl pH 7.5, 300 mM KCl, 2% glycerol, 1 mM β-mercaptoethanol, 1 mM PMSF, 1 mM DTT) at 4°C for 4 h. Then the dialysed fractions were supplemented with 1% Triton X-100 and loaded on a GSTrap HP column (GE Healthcare, Cat#: 17-5282-01). The column was washed with 25 ml wash buffer (40 mM Tris-HCl pH 7.5, 300 mM KCl, 2% glycerol, 1 mM β-mercaptoethanol, 1 mM PMSF, 1 mM DTT) and eluted with gradient elution buffer from 0 mM to 15 mM reduced glutathione (40 mM Tris-HCl pH 8.0, 300 mM KCl, 2% glycerol, 1 mM β -mercaptoethanol, 1 mM PMSF, 1 mM DTT). The peak fractions were collected and treated with thrombin (Calbiochem, Cat#: 605157-1KU) at 4°C overnight to remove the GST-6×His tag. The fractions were concentrated by 50 kDa molecular weight cut-off (MWCO) centricon (Millipore, Cat#: UFC905024), and loaded to HiLoad 26/600 Superdex 200 pg column (GE Healthcare). The gel filtration buffer contained 40 mM Tris-HCl pH 7.5, 300 mM KCl, 5 mM β -mercaptoethanol and 2 mM DTT. The peak fractions containing DCL1 were collected and dialysed with one litre dialysis buffer (20 mM Tris-HCl buffer pH 7.5, 40 mM KCl, 2 mM β -mercaptoethanol, 2 mM DTT, 50% glycerol) 4°C for 6 h. The final purified protein was quantified by SDS PAGE and aliquoted for storage at -80 °C.

For expression of recombinant proteins in E.coli., transformed BL21 DE3 cells were grown in Terrific Broth (TB) for recombinant CHR2 and its variants or in Luria Broth (LB) for recombinant SE and HYL1 proteins. Cells were grown at 37 °C until $\mathrm{OD}_{600\mathrm{nm}} = 0.6$. Expression of recombinant proteins was typically induced with 0.5 mM IPTG at 16 °C overnight.

For purification of HYL1, the induced bacterial cells were collected and re-suspended in lysis buffer (40 mM Tris-HCl buffer pH 8.0, 300 mM KCl, 2% glycerol, 1 mM β -mercaptoethanol, 1 mM PMSF, 1% Triton X-100) and disrupted with a high pressure homogenizer (AVESTIN). After centrifugation and filtration with 0.4- μm membrane, the cleared lysate was supplemented with 20 mM imidazole and loaded onto a HisTrap HP column (GE Healthcare, Cat#: 17-5248-02). The column was washed with 25 ml wash buffer (40 mM Tris-HCl pH 8.0, 300 mM KCl, 2% glycerol, 1 mM β -mercaptoethanol, 1 mM PMSF, 80 mM imidazole) and eluted with gradient elution buffer from 80 to 150 mM imidazole (40 mM Tris-HCl pH 8.0, 300 mM KCl, 2% glycerol, 1 mM β -mercaptoethanol, 1 mM PMSF). The peak fractions containing the recombinant 6×His-SUMO-HYL1 proteins were pooled and treated with SUMO protease at 4°C overnight to remove the 6×His-SUMO tag. The fractions were concentrated by 50 kDa molecular weight cut-off (MWCO) centricon (Millipore), and loaded onto a HiLoad 26/600 Superdex 200 pg column (GE Healthcare). The gel filtration buffer contained 20 mM Tris-HCl pH 7.4, 50 mM KCl, 2 mM β -mercaptoethanol and 2 mM DTT. The peak fractions containing HYL1 were collected and concentrated again by 50 kDa molecular weight cut-off (MWCO) centricon (Millipore). The HYL1 protein was supplemented with 50% glycerol and finally frozen by liquid nitrogen and stored at -80 °C.

For purification of $6\times$ His-SUMO-SE, the induced bacterial cells were collected and re-suspended in lysis buffer (20 mM Tris-HCl buffer pH 8.5, 300 mM KCl, 2% glycerol, 1 mM β -mercaptoethanol, 1 mM PMSF, 1% Triton X-100, 1 pellet per 50 ml Complete EDTA-free protease inhibitor (Roche)) and disrupted by the high pressure homogenizer (AVESTIN). After centrifuge and filtering (0.4 μ m filter), the cleared lysate was supplemented with 20 mM imidazole and loaded on a HisTrap HP column (GE Healthcare, Cat#: 17-5248-02). The column was washed with 25 ml wash buffer (20 mM Tris-HCl pH 8.5, 300 mM KCl, 2% glycerol, 1 mM

 β -mercaptoethanol, 1 mM PMSF, 80 mM imidazole) and eluted with gradient elution buffer from 80 to 150mM imidazole (20 mM Tris-HCl pH 8.5, 300 mM KCl, 2% glycerol, 1 mM β -mercaptoethanol, 1 mM PMSF). The peak fractions containing the recombinant $6\times$ His-SUMO-SE proteins were pooled and concentrated by 50 kDa molecular weight cut-off (MWCO) centricon (Millipore), and loaded onto a HiLoad 26/600 Superdex 200 pg column (GE Healthcare). The gel filtration buffer contained 20 mM Tris-HCl pH 8.5, 300 mM KCl and 5 mM β -mercaptoethanol. The peak fractions containing $6\times$ His-SUMO-SE were collected and dialysed with one litre dialysis buffer (20 mM Tris-HCl buffer pH 8.5, 150 mM KCl, 5 mM β -mercaptoethanol, 50% glycerol) at 4 °C for 6 h. The final purified protein was quantified by SDS-PAGE and aliquoted for storage at $-80\,^{\circ}\text{C}$.

For purification of GST-CHR2-957-1823aa-6×His, the induced bacterial cells were collected and re-suspended in lysis buffer (50 mM sodium phosphate buffer pH 8.0, 500 mM NaCl, 2% glycerol, 1 mM β -mercaptoethanol, 1 mM PMSF, 1% Triton X-100) and disrupted by the high pressure homogenizer (Avestin). After centrifugation and clearing with a 0.4-µm filter, the cleared lysate was supplemented with 20 mM imadazole and loaded onto a HisTrap HP column (GE Healthcare, Cat#: 17-5248-02). The column was washed with 25 ml wash buffer containing 80 mM imidazole, followed by 25 ml wash buffer containing 150 mM imidazole (50 mM sodium phosphate buffer pH 8.0, 500 mM NaCl, 2% glycerol; 1 mM β-mercaptoethanol, 1 mM PMSF). Then bound proteins were eluted with gradient elution buffer from 150 to 300 mM imidazole (50 mM sodium phosphate buffer pH 8.0, 500 mM NaCl, 2% glycerol; 1 mM β-mercaptoethanol, 1 mM PMSF). The peak fractions containing the recombinant GST-CHR2-957-1823aa-6×His proteins were pooled and dialysed with 2-l GST dialysis buffer (50 mM sodium phosphate buffer pH 7.6, 500 mM NaCl, 2% glycerol, 1 mM β-mercaptoethanol, 1 mM PMSF, 1 mM DTT) at 4 °C for 4 h. Then fractions were supplemented with 1% Triton X-100 and loaded onto a GSTrap HP column (GE Healthcare, Cat#: 17-5282-01). The column was washed with 25 ml wash buffer (50 mM sodium phosphate buffer pH 7.6, 500 mM NaCl, 2% glycerol, 1 mM β-mercaptoethanol, 1 mM PMSF, 1 mM DTT) and eluted with gradient elution buffer from 0 to 15 mM reduced glutathione (50 mM sodium phosphate buffer pH 8.0, 500 mM NaCl, 2% glycerol, 1 mM β -mercaptoethanol, 1 mM PMSF, 1 mM DTT). The peak fractions were collected and dialysed with one litre dialysis buffer (50 mM sodium phosphate buffer pH8.0, 500 mM NaCl, 5 mM β-mercaptoethanol, 2 mM DTT, 50% glycerol) at 4°C for 6 h. The final purified protein was quantified by SDS-PAGE and aliquoted for storage at -80 °C. The same purification protocol was applied for purification of CHR2 derivatives.

ATPase assay. The method for the ATPase assay was modified from a previous description²⁷. For Extended Data Fig. 2e, 1 pmol recombinant CHR2 or its derivatives were added into ATP hydrolysis reactions (20 µl) containing 20 mM sodium phosphate buffer pH 7.0, 25 mM KCl, 5 mM MgCl₂, 2 mM DTT, 500 ng dsDNA, $0.1\,\mu l\,\gamma^{-32}P$ ATP (PerkinElmer, 3,000 Ci/mmol). Note: the final pooled concentration tration of NaCl and KCl in the reaction systems was about 75 mM. Reactions were incubated at 37 °C for 2 h. For Fig. 5c and Extended Data Fig. 9g-i, the reactions were carried out in 20 mM Tris-HCl, pH 7.5, 5 mM MgCl $_2$, 2 mM DTT, 0.3% NP-40, 1 U/μl SUPERase-In RNase Inhibitor (for pri-miRNA stimulated ATPase assay, Thermo Fisher). The final pooled concentration of NaCl and KCl in the reaction systems was ~60 mM, of which 50 mM was from CHR2 protein dialysis buffer and 10 mM was from dsDNA or pri-miRNA-dissolved buffer. 40 nM recombinant CHR2 or its derivatives was pre-incubated with dsDNA fragment (the same as in dsDNA EMSA) or with annealed pri-miR166f for 10 min before addition of 50 nM γ -³²P ATP and 100 nM cold ATP. Reactions were incubated at 37 °C for the indicated time points. Reactions were stopped by addition of 12.5 mM EDTA and 2.5 mM cold ATP and being placed on ice. For measurement of the substrate-regulated ATPase activity, 0.5 μM dsDNA or 1 μM pri-miR166f were added to the reactions. Liberated phosphate was analysed by thin layer chromatography (TLC) and phosphorimaging. The images were quantified with ImageQuant TL (GE Healthcare) and the ATP hydrolysis rates of CHR2 and its ATPase mutant were calculated using the data of 60 min reaction for Fig. 5c.

In vitro transcription and 5' labelling of RNA/DNA. In vitro transcription and 5' labelling of RNA/DNA substrates including pri-miR166f were performed as described 12 . The substrate of 5' labelled dsDNA for EMSA is a PCR fragment containing the T7 promoter followed by the pri-miR166f sequence. The 5' labelled ssDNA is a synthesized primer: 5'-(A) $_{97}$ CCCTATAGTGAGTCGTATTA-3'. The substrate of 5' labelled single-stranded (ss)RNA is an ssRNA (100 nt) in vitro transcribed using T7-G3A97_Rev primer 42 as a template.

In vitro Microprocessor assay. We added 1 pmol recombinant DCL1, 2 pmol HYL1, 2 pmol SE, 0.5 pmol CHR2 or its derivatives and 1,000 counts per minute (c.p.m.) of RNA substrate to 30 μ l assay buffer containing 20 mM Tris-HCl pH7.5, 50 mM KCl, 4 mM MgCl₂, 1 mM DTT, 5 mM ATP, 1 mM GTP and 1 U/ μ l SUPERase-In RNase Inhibitor (Thermo Fisher). The final pooled concentration of NaCl and KCl was ~70 mM, of which ~20 mM salt was from protein dialysis buffer and RNA-dissolved buffer. The reconstitution assay was carried

out at 37 °C. The reactions were stopped by adding 1 volume TBE-Urea sample buffer (Bio-Rad), being heated at 95 °C for 10 min and then being chilled on ice. The DCL1-processed products were fractionated using 10% denaturing polyacrylamide gel and detected overnight with a phosphor imaging plate (GE Healthcare). The images were quantified with Gel-Pro Analyzer (Media Cybernetics) software.

Electrophoretic mobility shift assays. Recombinant proteins and labelled RNA or DNA were mixed in the EMSA buffer (20 mM Tris-HCl pH 7.5, 2 mM MgCl₂, 2 mM DTT, 5 mM ATP, 0.3% NP-40, 1 U/μl SUPERase-In RNase Inhibitor (for RNA EMSA, Thermo Fisher)). The final pooled concentration of NaCl and KCl was ~55 mM, of which 50 mM was from protein dialysis buffer and 5 mM from DNA- or RNA-dissolved buffer. Mixtures were incubated at room temperature for 30 min. Bound complexes were resolved on native 1% agarose gel and visualized by radiography. The images were quantified with Gel-Pro Analyzer (Media Cybernetics) software. The K_d for SE and HYL1 and apparent K_d for CHR2 and its variants were calculated using Prism 5 (GraphPad) software. For the modelling prediction for the CHR2-nucleic acid binding pattern, the original data were analysed with GraphPad Prism 5^6 ; specific binding with a Hill slope model was the best fit. UV-crosslinking and ribonucleoprotein immunoprecipitation. Three-week-old plants grown on soil were irradiated four times with UV at 150 mJ/cm². The fixed samples were ground in liquid nitrogen and nuclei were isolated using a chromatin immunoprecipitation (ChIP) protocol as described⁴⁷. The nuclei extracts were diluted with RIP buffer (40 mM Tris-HCl pH 7.5, 100 mM KCl, 5 mM MgCl₂, 5 mM DTT, 0.2% Triton X-100, 2% glycerol, 1 mM PMSF, 25 μM MG132, 1 pellet per 10 ml Complete EDTA-free protease inhibitor (Roche) with 10 U/ml TURBO DNase (Thermo Fisher)) and immunoprecipitated with an anti-c-Myc agarose (Sigma, Cat#: A7470) at 4 °C for 4 h. Immunoprecipitates were washed three times with RIP buffer and once with high salt buffer (40 mM Tris-HCl pH 7.5, 500 mM KCl, 5 mM MgCl₂, 5 mM DTT, 0.2% Triton X-100, 2% glycerol, 1 mM PMSF, 25 μM MG132, 1 pellet per 10 ml Complete EDTA-free protease inhibitor (Roche)) at 4°C for 5 min, followed by two washes with the proteinase K buffer (100 mM Tris-HCl pH 7.5, 50 mM NaCl, 10 mM EDTA). The beads were treated with Proteinase K (4 mg/ml) in 150 μ l Proteinase K buffer at 37 °C for 20 min. After treatment with Proteinase K, the RNA was extracted using TRI Reagent (Sigma) and treated with TURBO DNase (Thermo Fisher). One half of the RNA was directly used for RT-qPCR. The other half (as a control) was further treated with RNase A (Sigma) and RNase T1 (Thermo Fisher) before RT-qPCR.

dsDNA and pri-miRNA remodelling/unwinding assays. For the pri-miRNA substrate, a 5' 32P labelled 26-nt RNA fragment was annealed to a truncated strand of pri-miR166f to generate a nicked pri-miR166f (Extended Data Fig. 9b). For the dsDNA substrate, a 5' 32P labelled 19-nt ssDNA fragment was annealed to a long ssDNA fragment to generate a dsDNA with long 5' overhang (Extended Data Fig. 9e). The sequences of primers used to make dsDNA or pri-miRNA are listed in Supplementary Table 4. Recombinant CHR2 or its derivatives and annealed dsDNA or pri-miRNA were mixed in the remodelling buffer (20 mM Tris-HCl pH 7.5, 5 mM MgCl₂, 2 mM DTT, 10 mM ATP, 1 mM GTP, 0.3% NP-40, 1 U/μl SUPERase-In RNase Inhibitor (specific for the pri-miRNA remodelling assay)). The final pooled concentration of NaCl and KCl was ~55 mM, of which 50 mM was from CHR2 protein dialysis buffer and 5 mM from dsDNA- or RNA-dissolved buffer. Before protease K treatment, the reactions were incubated at 37 °C (for DNA) or 25 °C (for RNA) for the indicated times. The ssDNA and dsDNA or RNA were fractionated using 15% (for DNA) and 12% (for RNA) native PAGE. The signals were detected by radiography. The images were quantified with ImageQuant TL (GE Healthcare).

In vivo DMS modification. For primer extension assays to probe in vivo RNA folding, approximately 3 g three-week-old $\mathit{hyl1-2~chr2-1;PCHR2-gCHR2-FM}$ and $\mathit{hyl1-2~chr2-1a}$ plants grown on soil were collected and completely covered in 20 ml 1× DMS reaction buffer (40 mM HEPES pH 7.5, 100 mM KCl and 0.5 mM MgCl₂) in a 50-ml Corning tube. DMS (Sigma, Cat#: D186309) was added to a final concentration of 0.75% as described²⁸. Mock treatment was performed by addition of deionized water. Samples were treated in the DMS reaction buffer or mock solution at room temperature under a vacuum condition. Different time courses were initially tested; finally, a period of 30 min was found to be the optimal incubation time for adult plants (Extended Data Fig. 11c). To quench the reaction, 5 ml β -mercaptoethanol was added to a final concentration of 20%, and the mixture was incubated for 2 min under vacuum. After washing 4 times with 50 ml deionized water, the samples were immediately frozen with liquid N_2 and ground into powder.

For target-specific DMS–MaPseq, three-week-old Col-0 and *chr2-1* plants grown on soil were collected and treated with or without DMS using the same conditions as above except for DMS concentration. Several dosages of DMS were also tested; eventually 1% DMS was chosen for the assay because plant materials turned brown under treatment with 5% and 1.5% DMS and total RNA appeared to decay under these conditions.

Nuclear RNA extraction. Nuclear RNA extraction was performed as described 48 . In brief, 0.3 g ground powder was dissolved in 5 ml lysis buffer (20 mM HEPES pH7.5, 20 mM KCl, 2.5 mM MgCl $_2$, 25% glycerol, 250 mM sucrose, 5 mM DTT, 1 U/10µl RNase inhibitor (Thermo Fisher) and 1× Proteinase inhibitor cocktail without EDTA (Roche)). The homogenate was filtered through a double layer of Miracloth. The flow-through was centrifuged at 1,500g for 10 min at 4 $^{\circ}$ C. After removal of supernatant, the pellet was washed twice with 5 ml nuclear resuspension buffer (20 mM HEPES pH 7.5, 2.5 mM MgCl $_2$, 25% glycerol, 0.2% Triton X-100, 20 μ RNase inhibitor (Thermo Fisher)). Then the total nuclear RNA was extracted using TRI Reagent (Sigma).

Primer extension assays for probing in vivo RNA folding. Probing of in vivo RNA secondary structure by primer extension assay was performed as described²⁸ with modifications. For each sample, 2 µg total nuclear RNA was treated with TURBO DNase (Thermo Fisher), followed by phenol-chloroform extraction. DNasetreated nuclear RNA was mixed with ~200,000 c.p.m. ³²P-radiolabelled genespecific primer (Supplementary Table 4). The mixture was precipitated by ethanol and resuspended in 10 μ l Tris-KCl solution (10 mM Tris-HCl pH 7.5 and 50 mM KCl). The solution was heated at 75 °C for 3 min, followed by incubation at 35 °C (for 18S rRNA) or 55 °C (pri-miR164b) for 15 min. 10 μl reverse transcription reaction buffer mixed with 1 mM DTT, 1 mM dNTPs, 1 μ l RNase Inhibitor (Thermo Fisher) and 1 µl SuperScript III (for 18S rRNA) (Thermo Fisher) or SuperScript IV (for pri-miR164b) reverse transcriptase (Thermo Fisher) was added. The reaction proceeded for 1 h at 55 °C (for 18S rRNA) or 60 °C (for pri-miR164b). To stop the reaction and hydrolysation of RNA, 2 µl of 2 M NaOH was added and mixture was heated at 95 °C for 10 min. After neutralization by 5 M HCl, the mixture was phenol-chloroform extracted and precipitated. Then the cDNA was resuspended in loading buffer (95% deionized formamide, 0.025% bromophenol blue, 0.025% xylene cyanol, 5 mM EDTA and 0.025% SDS) and size fractionated on 8% denaturing polyacrylamide gel. Gel image was collected with a Typhoon FLA7000 (GE Healthcare) and bands were quantified using ImageQuant TL (GE Healthcare).

Target-specific DMS-MaPseq. Target-specific DMS-MaPseq was performed as described $^{\!29}\!.$ For each sample, 5 μg DNase-treated nuclear RNA was mixed with gene-specific RT primers (5 pmol each primer, up to 5 gene-specific primers in one reaction, Supplementary Table 4). The mixture was precipitated and resuspended in 10 µl Tris-KCl solution (10 mM Tris-HCl pH 7.5 and 50 mM KCl). The solution was heated at 75 °C for 3 min, followed by incubation at 57 °C for 15 min. Four microlitres 5× First-Strand buffer (250 mM Tris-HCl pH 8.3, 375 mM KCl, 15 mM MgCl₂), 1 μl 0.1 M DTT (prepared freshly), 1 μl RNase inhibitor (Thermo Fisher), 1 μl H2O and 1 μl TGIRT-III (Ingex, Cat#: TGIRT50) were added. The mixture was then incubated at room temperature for 30 min. Then 2 μl 10 mM dNTP was added and the reverse transcription proceeded at 63 °C for 2.5 h. The reaction was stopped by adding 2 µl of 2.5 M NaOH and heating at 95 °C for 3 min. After neutralization by 5 M HCl, the mixture was phenol-chloroform extracted and applied to an illustra MicroSpin S-200 HR column (GE Healthcare) to remove RT primers and nucleotides. The cleaned cDNA was precipitated and resuspended in deionized water. Then pri-miRNAs were amplified using KOD hot start DNA polymerase (Millipore) with gene-specific primers (Supplementary Table 4). PCR bands were gel purified and normalized according to band intensity before library construction.

PCR products were mixed equally and fragmented into 50–200 bp using NEBNext dsDNA Fragmentase (NEB) following the manufacturer's protocol. After purification using QIAquick nucleotide removal kit (QIAGEN), the fragments were subjected to end repair, adenylation and adaptor ligation using Illumina adapters, mainly following the published protocol⁴⁹. The fragments were barcoded through adaptor ligation. The ligation products were size fractionated on 3% low melting agarose gel, and 250–350 bp adaptor-ligated fragments were purified by gel excision. Next, the purified barcoded libraries were enriched by 12 cycles of PCR using KOD hot start DNA polymerase. Finally, the PCR products were cleaned using Agencourt AMPure XP beads (Beckman). The libraries were quantified using Agilent TapeStation before sequencing by 150 bp single-end reads on the Illumina NextSeq 500 at Texas A&M University.

Sequencing alignment and analysis. Raw fastq files were initially filtered for a quality control that requires a quality score >30 by sickle (https://github.com/ucdavis-bioinformatics/sickle) and trimmed to remove the adaptor sequences by Cutadapt⁵⁰. Clean reads over 35 bp were retained. Reads were aligned using Burrows-Wheeler Aligner (BWA)⁵¹ allowing 5% mismatches with the settings: bwa aln -n 0.05. The mapping results were sorted by Picard tools (http://broadinstitute. github.io/picard/) with coordination and the base calls of aligned reads to the reference sequence were summarized using samtools (v1.5) mpileup⁵². Nucleotide mismatches and sequencing depth were extracted using sequenza-utils (v2.1) pileup2acgt (https://pypi.python.org/pypi/sequenza-utils). The DMS signal was calculated as number of mismatches per sequencing depth for each adenine (A) and cytosine (C) nucleotide. The two biological replicates were normalized to the

identical means of total DMS signal. Then the average DMS signal for each A and C nucleotide was calculated. Based on the DMS signal, the secondary structures of pri-miRNAs were modelled by RNAfold⁵³. The threshold was used to separate adenine and cytosine bases into paired and unpaired nucleotides to produce the best fitting model for our experimental data. The threshold constraint varied between 0.01 to 0.03 depending on different pri-miRNAs. DMS signals were colour coded on structure models using VARNA⁵⁴ (http://varna.lri.fr,).

Quantification and statistical analysis. The images of Microprocessor activity and sRNA blot assays were quantified with Gel-Pro Analyzer (Media Cybernetics). The $K_{\rm d}$ for EMSA assays was calculated using Prism 5 (GraphPad) software. The images from primer extension assays, dsDNA and pri-miRNA remodelling/helicase assays and ATPase assays were quantified with ImageQuant TL (GE Healthcare). Unpaired, two-tailed Student's t-test was performed using the software Excel. All statistics are described below unless specifically mentioned in the Figures or Figure legends.

For Figs. 3, 5d, quantification of the Microprocessor cleavage efficiency was calculated by the ratio of processed to unprocessed pri-miR166f fragments. The relative efficiency was normalized to that of the Microprocessor reaction alone where the ratio was arbitrarily set at 1 with s.d. from three replicates.

For Fig. 4d, the relative signal of pri-miRNAs was normalized initially to the input and then to the control immunoprecipitate, where the ratio was arbitrarily set to 1 with s.d. from three biological repeats (*P < 0.05; **P < 0.01; unpaired, two-tailed Student's t-test).

For Fig. 5e, f and Extended Data Figs. 11e–h, 12, in the primer extension assays, the colour intensity of coded nucleotides along the pri-miR164b illustrates the relative DMS reactivity, calculated as the band signal intensity normalized to the highest level, which was set arbitrarily to 1.0. DMS (+/-) refers to the DMS treated and untreated samples, respectively. In the DMS–MaPseq analysis, DMS mutation frequencies of A and C residues (mismatch/total) from targeted pri-miRNAs averaged from two biological replicates were plotted along pri-miRNAs equence. Position 1 corresponds to the 5^\prime end of modelled regions. The overall and zoomed-in secondary structures of the targeted pri-miRNAs were modelled from DMS activity according to RNAfold 53 . The nucleotides that displayed different DMS activity on pri-miRNAs between Col-0 and chr2-1 plants are colour-coded.

For Extended Data Figs. 4, previously published datasets^{55–58} were reanalysed. **Graph drawing.** Graphs with dot plots (individual data points) were drawn using GraphPad Prism 7.

Reporting summary. Further information on experimental design is available in the Nature Research Reporting Summary linked to this paper.

Data availability. Original data that support the findings of this study are available from the corresponding author upon reasonable request. The GEO accession numbers for sRNA sequence and DMS–MaPseq are GSE108858 and GSE108857, respectively. Source Data for graphs plotted in Figs. 1, 3–5 are available in the online version of this paper. Gel source data for Figs. 1, 2, 4, 5, Extended Data Figs. 1–5, 8–11 are available in Supplementary Fig. 1.

- Zhang, X., Henriques, R., Lin, S. S., Niu, Q. W. & Chua, N. H. Agrobacterium-mediated transformation of *Arabidopsis thaliana* using the floral dip method. *Nat. Protocols* 1, 641–646 (2006).
- 39. Zhu, H. et al. *Arabidopsis* Argonaute10 specifically sequesters miR166/165 to regulate shoot apical meristem development. *Cell* **145**, 242–256 (2011).
- Zhao, B. et al. Structural basis for concerted recruitment and activation of IRF-3 by innate immune adaptor proteins. *Proc. Natl Acad. Sci. USA* 113, E3403–E3412 (2016).
- Yoo, S. D., Cho, Y. H. & Sheen, J. Arabidopsis mesophyll protoplasts: a versatile cell system for transient gene expression analysis. Nat. Protocols 2, 1565–1572 (2007).
- Zhang, Z. et al. RISC-interacting clearing 3'- 5' exoribonucleases (RICEs) degrade uridylated cleavage fragments to maintain functional RISC in Arabidopsis thaliana. eLife 6, e24466 (2017).
- Raabe, C. A., Tang, T. H., Brosius, J. & Rozhdestvensky, T. S. Biases in small RNA deep sequencing data. *Nucleic Acids Res.* 42, 1414–1426 (2014).
- 44. Sorefan, K. et al. Reducing ligation bias of small RNAs in libraries for next generation sequencing. *Silence* **3**, 4 (2012).
- Shen, S. et al. rMATS: robust and flexible detection of differential alternative splicing from replicate RNA-Seq data. Proc. Natl Acad. Sci. USA 111, E5593–E5601 (2014).
- Du, Z., Zhou, X., Ling, Y., Zhang, Z. & Su, Z. agriGO: a GO analysis toolkit for the agricultural community. *Nucleic Acids Res.* 38, W64–W70 (2010).
- Gendrel, A. V., Lippman, Z., Martienssen, R. & Colot, V. Profiling histone modification patterns in plants using genomic tiling microarrays. *Nat. Methods* 2, 213–218 (2005).
- Zhang, Z. et al. KETCH1 imports HYL1 to nucleus for miRNA biogenesis in Arabidopsis. Proc. Natl Acad. Sci. USA 114, 4011–4016 (2017).
- Feng, S., Rubbi, L., Jacobsen, S. E. & Pellegrini, M. Determining DNA methylation profiles using sequencing. *Methods Mol. Biol.* 733, 223–238 (2011).
- Martin, M. Cutadapt removes adapter sequences from high-throughput sequencing reads. EMBnet J. 17, 10–12 (2011).



- 51. Li, H. & Durbin, R. Fast and accurate short read alignment with Burrows-Wheeler transform. *Bioinformatics* **25**, 1754–1760 (2009).
- 52. Li, H. et al. The Sequence Alignment/Map format and SAMtools. *Bioinformatics* **25**, 2078–2079 (2009).
- 53. Lorenz, R. et al. ViennaRNA Package 2.0. Algorithms Mol. Biol. **6**, 26 (2011).
- Darty, K., Denise, A. & Ponty, Y. VARNA: Interactive drawing and editing of the RNA secondary structure. *Bioinformatics* 25, 1974–1975 (2009).
- Li, C. et al. Concerted genomic targeting of H3K27 demethylase REF6 and chromatin-remodeling ATPase BRM in Arabidopsis. Nat. Genet. 48, 687–693 (2016).
- Bezhani, S. et al. Unique, shared, and redundant roles for the Arabidopsis SWI/SNF chromatin remodeling ATPases BRAHMA and SPLAYED. Plant Cell 19, 403–416 (2007).
- Tang, X. et al. The *Arabidopsis* BRAHMA chromatin-remodeling ATPase is involved in repression of seed maturation genes in leaves. *Plant Physiol.* 147, 1143–1157 (2008).
- Archacki, R. et al. BRAHMA ATPase of the SWI/SNF chromatin remodeling complex acts as a positive regulator of gibberellin-mediated responses in Arabidopsis. PLoS One 8, e58588 (2013).

- Allen, R. S. et al. Genetic analysis reveals functional redundancy and the major target genes of the *Arabidopsis* miR159 family. *Proc. Natl Acad. Sci. USA* 104, 16371–16376 (2007).
- 60. Raman, S. et al. Interplay of miR164, CUP-SHAPED COTYLEDON genes and LATERAL SUPPRESSOR controls axillary meristem formation in *Arabidopsis thaliana*. *Plant J.* **55**, 65–76 (2008).
- Archacki, R. et al. Arabidopsis SWI/SNF chromatin remodeling complex binds both promoters and terminators to regulate gene expression. Nucleic Acids Res. 45, 3116–3129 (2017).
- Laubinger, S. et al. Dual roles of the nuclear cap-binding complex and SERRATE in pre-mRNA splicing and microRNA processing in *Arabidopsis* thaliana. Proc. Natl Acad. Sci. USA 105, 8795–8800 (2008).
- Raczynska, K. D. et al. The SERRATE protein is involved in alternative splicing in Arabidopsis thaliana. Nucleic Acids Res. 42, 1224–1244 (2014).
- Knop, K. et al. Active 5' splice sites regulate the biogenesis efficiency of *Arabidopsis* microRNAs derived from intron-containing genes. *Nucleic Acids Res.* 45, 2757–2775 (2017).
- Manavella, P. A. et al. Fast-forward genetics identifies plant CPL phosphatases as regulators of miRNA processing factor HYL1. Cell 151, 859–870 (2012).